Reprinted from Journal of the Optical Society of America A

Halo phenomena modified by multiple scattering

Yoshihide Takano and Kuo-Nan Liou

Department of Meteorology/Center for Atmospheric and Remote Sounding Studies, The University of Utah, Salt Lake City, Utah 84112

Received July 24, 1989; accepted November 16, 1989

Halo phenomena produced by horizontally oriented plate and column ice crystals are computed. Owing to the effect of multiple scattering, a number of optical features, in addition to the well-known halos and arcs caused by single scattering, can be produced in the sky. These include the 44° parhelion, the 66° parhelion, the anthelion, the uniform and white parhelic circle, and the uniform and white circumzenithal circle in the case of horizontally oriented plates. The anthelion is a result of double scattering that involves horizontally oriented columns that produce the Parry arc. The optical phenomena identified in the present study are compared with those of previous research and discussed.

INTRODUCTION

Various halo phenomena have been calculated by several researchers.[1–4] Using the Monte Carlo approach, Tränkle and Greenler[5] discussed multiple-scattering effects on halo phenomena. In this paper we demonstrate the effect of multiple scattering on halo phenomena produced by horizontally oriented hexagonal ice crystals. The geometric ray-tracing and radiative-transfer schemes developed by Takano and Liou[6,7] are used in the calculations. For the identification of halo positions, it is sufficient to include geometric optic rays undergoing reflections and refractions. In the present study, light rays that undergo seven internal reflections are accounted for in the computation. Although the theoretical foundation for the computation is the same as in our previous research, this paper focuses on the discussion of the ice crystal optical phenomena. The tip angles of the horizontally oriented crystals are assumed to be 0°; thus the resulting optical phenomena may be exaggerated. Nevertheless, the computed result can be used as a guide to understanding the physical mechanism for the formation of various halos and arcs.

In Section 2, halo phenomena produced by horizontally oriented plates and columns are described, and unresolved problems related to halos are discussed. In Section 3, concluding remarks are given.

HALOS PRODUCED BY HORIZONTALLY ORIENTED ICE CRYSTALS

Two-Dimensional Plates

Figure 1 shows the scattering geometry for horizontally oriented plate crystals [referred to as two-dimensional (2-D) plates]. Even though there is considerable multiple scattering, all the scattered light is confined to four latitude belts ($\theta = \pm\theta_0$ and $\theta = \pm\theta^*$) in the case of 2-D plates. In this diagram, θ_0 is the solar zenith angle and θ is the zenith angle at which the circumzenithal or circumhorizontal arcs are located. On the basis of ray-tracing geometry for 2-D plates, the zenith angle θ^* may be computed from the incoming solar zenith angle θ_0 in the form

$$\theta^* = \begin{cases} \pi/2 - \sin^{-1}(m_r^2 - \sin^2\theta_0)^{1/2} & \text{for } \theta_0 > \sin^{-1}(m_r^2 - 1)^{1/2} \simeq 58° \\ \sin^{-1}(m_r^2 - \cos^2\theta_0)^{1/2} & \text{for } \theta_0 < \cos^{-1}(m_r^2 - 1)^{1/2} \simeq 32° \end{cases}. \quad (1)$$

The scattered light associated with each latitude belt can be expressed only as a function of the azimuth angle, $\phi - \phi_0$, shown in Fig. 1.

Figure 2(a) shows the intensity of sunlight transmitted by 2-D plates with a length-to-width ratio ($L/2a$) of 0.4 along the latitude belt where the parhelic circle is located. The intensity due to single scattering is also shown in the lower part of this figure. The optical depth, τ, is a mean value averaged over the zenith angle θ. Even for a small optical depth of 1/8, the 44° parhelion (44°P) and anthelion (AN) due to the effect of the double scattering are produced. The 66° parhelion (66°P) can be clearly seen at $\phi - \phi_0 \simeq 72°$, owing to the effect of tertiary scattering. If $L/2a$ is close to 1, it will become more brilliant. This corresponds to the parhelia BB, reported by Ripley and Saugier.[8] There is also a faint peak at $\phi - \phi_0 \simeq 96°$. This peak should be referred to as the 22° parhelion of the 120° parhelion, rather than the 88° parhelion, since there is also a faint companion peak at $\phi - \phi_0 \simeq 144°$ produced by double scattering. When $\tau \gtrsim 8$, all the bright spots fade away and a white and uniform parhelic circle appears.

Figure 2(b) shows the intensity of sunlight transmitted by 2-D plates along the latitude belt where the circumzenithal arc is located. When the optical depth reaches 32, the intensity of transmitted sunlight is independent of the azimuth angle $\phi - \phi_0$. A uniform and white circumzenithal circle will appear in the blue sky instead of the colored circumzenithal arc that is usually observed.

Parry Columns

We consider here column crystals that have both their major axes and a pair of prism faces horizontal (referred to as Parry columns). Figure 3 shows the intensity distribution due to

0740-3232/90/050885-05$02.00

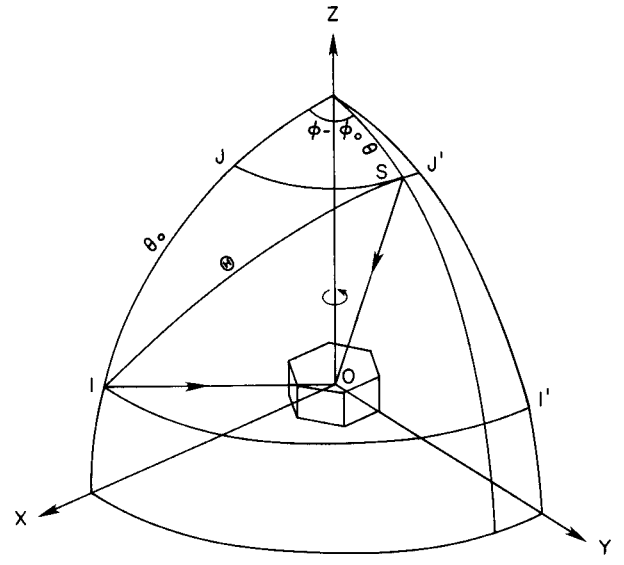

Fig. 1. Scattering geometry for 2-D plates. *IO* and *SO* denote the incident and scattered directions, respectively. All the scattered light is confined to the latitude belts *II'* and *JJ'* and their mirror images with respect to the horizontal plane *XOY*.

single scattering for Parry columns with $L/2a = 2.5$ for $\theta_0 = 73°$ by means of the equidistant projection. The angular resolutions are 2° for both the zenith angle θ and the azimuth angle $\phi - \phi_0$. Above the horizon there is no anthelion at the anthelic point (ATP), i.e., the point at $\phi - \phi_0 = 180°$ along the parhelic circle in Fig. 3(a). Below the horizon the antisolar peak (ASP) and a remarkably bright subsun (SS) are shown [Fig. 3(b)]. The antisolar peak results from rays that undergo two internal reflections (see Ref. 9).

The scattered light is confined to restricted areas in space in the case of Parry columns. Hence only the intensity of the sunlight as a function of the azimuth angle $\phi - \phi_0$ along the latitude belt of the parhelic circle is presented. This representation is shown in Fig. 4. In Fig. 4(a) a conspicuous anthelion (AN) appears owing to double scattering, even for a small optical depth of 1/8. Except for the anthelion, other features produced by multiple scattering remain the same as those produced by single scattering. This anthelion is caused by the subsun of the antisolar peak or the antisolar peak of the subsun. However, in the case of a higher solar elevation θ_0 of 30° the intensity patterns of transmitted sunlight for various optical depths are identical to those produced by single scattering. (For example, the peak at $\phi - \phi_0 \simeq 73°$ is the Parry arc crossing the parhelic circle.) This is because the subsun and the antisolar peak (subanthelion) become fainter for small solar zenith angles. In fact, the product of the scattering intensities of the subsun and the antisolar peak for $\theta_0 = 73°$ is greater than that for $\theta_0 = 30°$ by more than 1 order of magnitude. According to the statistics of the observed anthelion compiled by Lynch and Schwartz,[10] the anthelion has not been reported when the solar zenith angle is less than 44°. Our computed results are consistent with the observations. As demonstrated in the present study, the anthelion is produced by Parry columns, not by oriented columns as suggested by Lynch and Schwartz.[10] The deficiency of their explanation of the origin of the anthelion has been pointed out by Greenler.[2]

In addition, the intensity pattern of the parhelic circle in Fig. 4(a) shows a discontinuity at the azimuth angle $(\phi - \phi_0)$ of 124°. This reduction in intensity results from the absence of total reflection for the internally reflected rays. As in the case of 2-D plates, the critical angle $(\phi - \phi_0)$ for the total reflection, from simple geometry, is given by

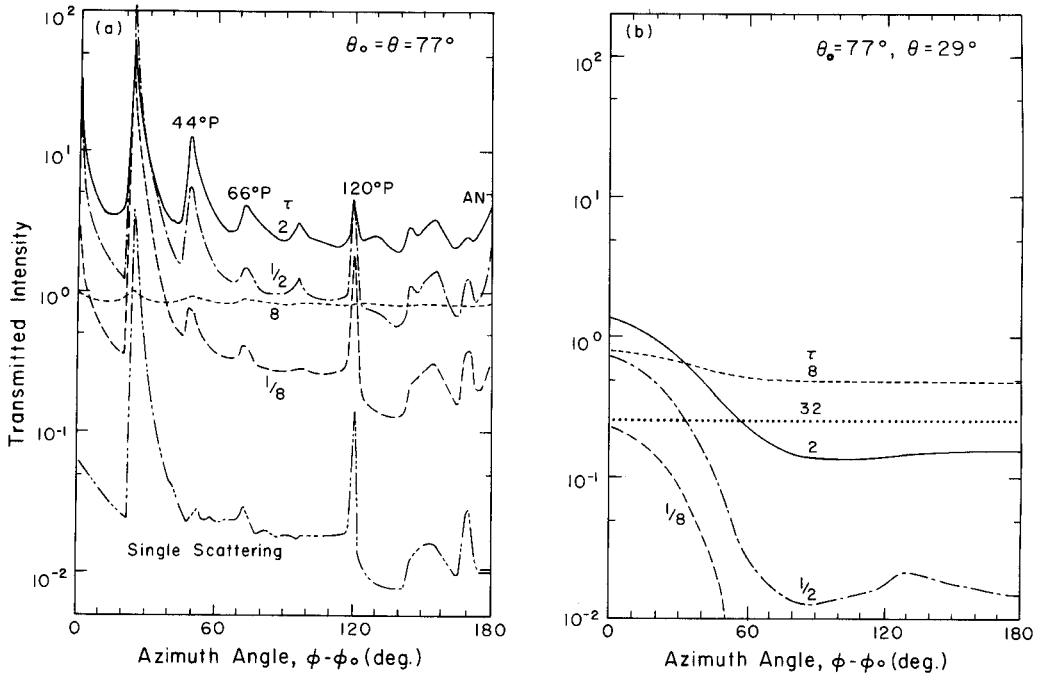

Fig. 2. Intensity of the sunlight transmitted by 2-D plates with $L/2a = 0.4$ along the latitude belt of (a) $\theta = 77°$ and (b) $\theta = 29°$ at a wavelength of 0.55 μm. The solar zenith angle $\theta_0 = 77°$. In (a) the intensity due to single scattering is also shown on a different scale. When the optical depth becomes 32 in (a), the intensity takes a constant value of 6.7×10^{-4}, which is not in the figure.

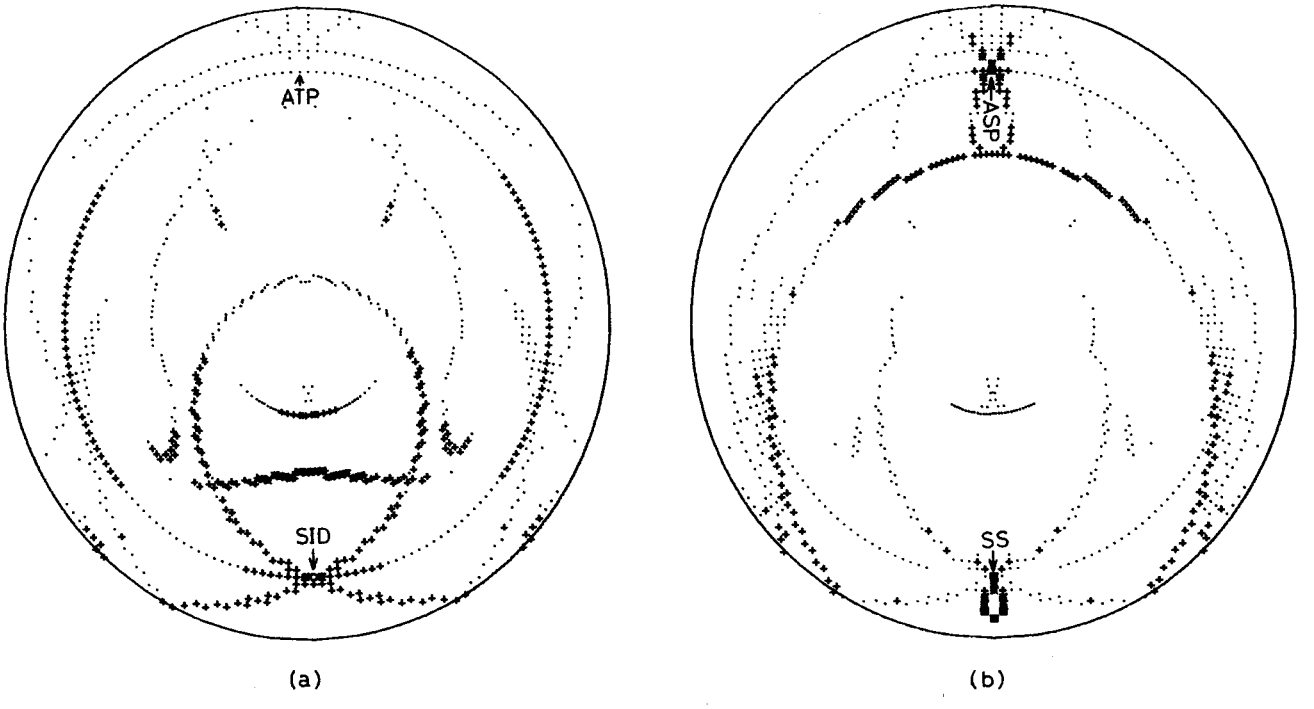

Fig. 3. Intensity distribution for Parry columns with $L/2a = 2.5$ at $\lambda = 0.55$ μm (a) above the horizon and (b) below the horizon. The solar zenith angle θ_0 is 73°. ·, +, *, and ■ denote 0, 1, 2, and 3, respectively, in units of $[\log_{10} P_{11}]$, where P_{11} is the relative intensity and [ ] denotes the integral part. SID, the solar incident direction.

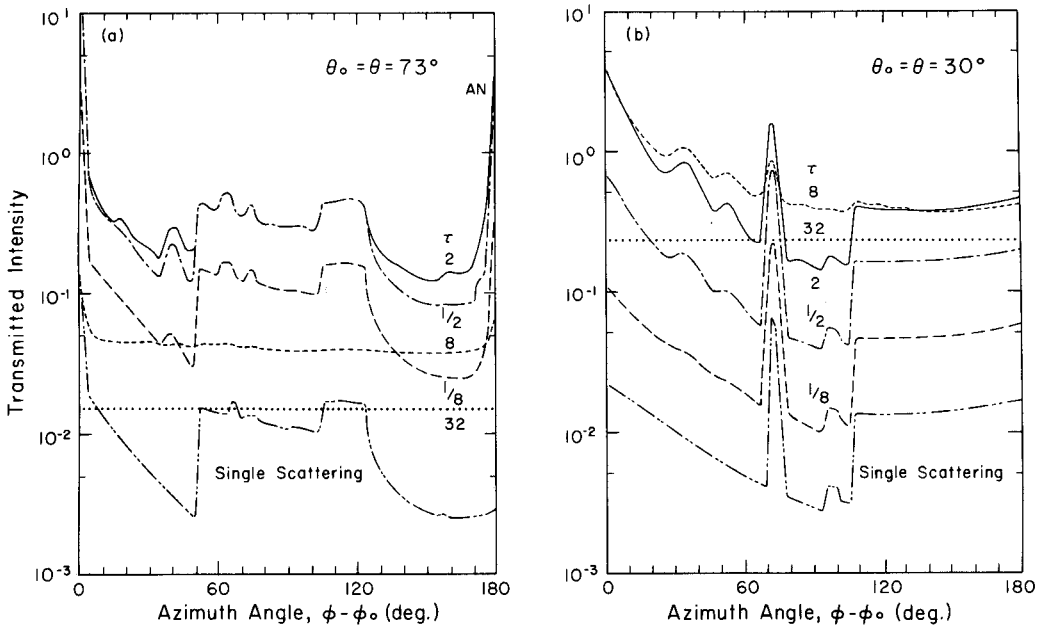

Fig. 4. Intensity of the sunlight transmitted by Parry columns with $L/2a = 2.5$ as a function of the azimuth angle $\phi - \phi_0$ for (a) $\theta_0 = \theta = 73°$ and (b) $\theta_0 = \theta = 30°$. The intensity due to single scattering is also shown in the lower part of the figure on a different scale.

$$(\phi - \phi_0)_c = 2 \sin^{-1}[(m_r^2 - 1)^{1/2}/\sin \theta_0]. \quad (2)$$

For $\theta_0 = 73°$, which is used in the present calculations, we find that $(\phi - \phi_0)_c = 124.5°$. According to Table 25 of Liljequist,[11] the observed parhelic circle can often be seen up to the azimuthal angle of approximately 120° when the solar zenith angles are within approximately 70° to 76°. The observed positions of the parhelic circle are in general agreement with the prediction based on Eq. (2).

Two-Dimensional Columns

Column crystals that orient with their major axes horizontal, as well as with random rotational orientation about the major axes (referred to as 2-D columns), produce no anthelion owing to the effect of double scattering. This is because the scattered light produced by 2-D columns spreads out more isotropically and because the intensities of the subsun and antisolar peak are weaker, as shown in Fig. 5(b), than those in Fig. 3(b). Instead, the anthelion appears, owing to the

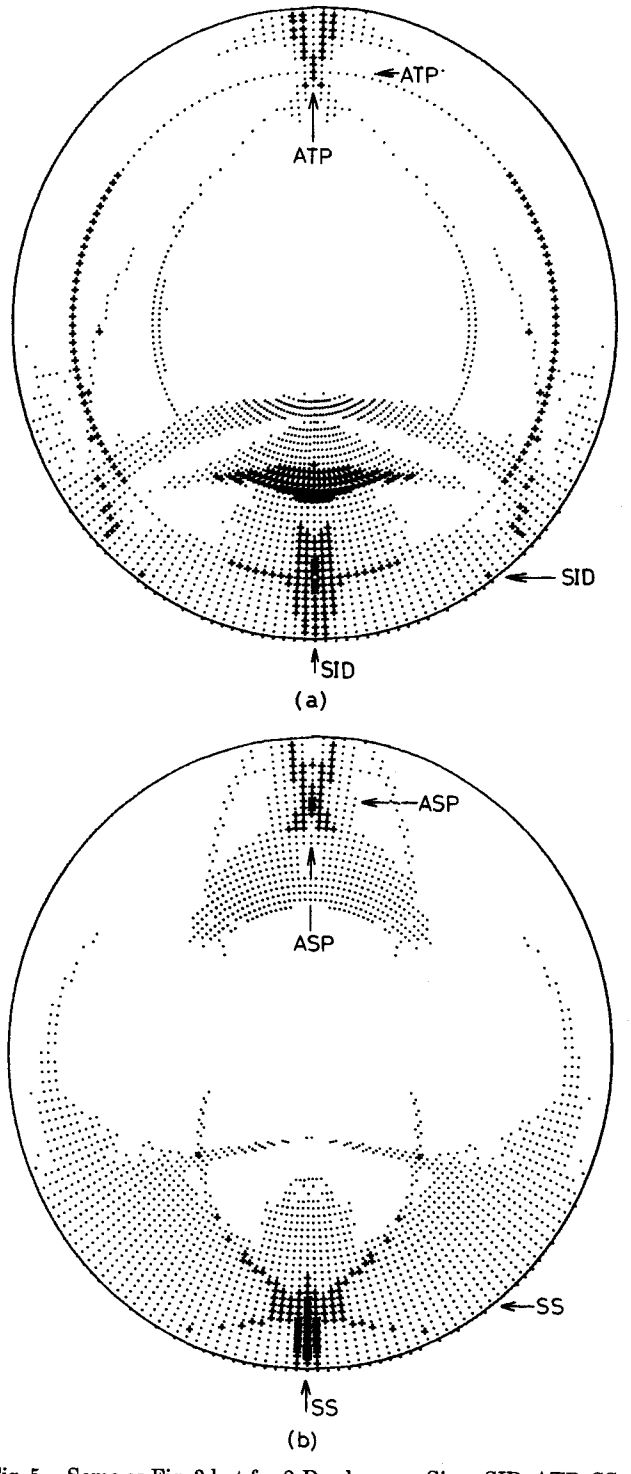

Fig. 5. Same as Fig. 3 but for 2-D columns. Since SID, ATP, SS, and ASP cannot be pinpointed exactly, arrows are used to indicate these positions.

combined brightness of the parhelic circle and the anthelic arcs at their common point of intersection, as shown in Fig. 5(a) (also see Greenler and Tränkle[4] and Humphreys[12]).

There is one important difference between Fig. 5(a) in this paper and Fig. 4(a) in the paper of Tränkle and Greenler.[5] In this study we show a broad maximum pattern around the light source that was not presented in their diagram. This pattern is caused mainly by externally reflected rays and results from the factor $1/\sin\Theta$ in the equation for the computation of the scattering phase function developed by Takano and Jayaweera,[9] where Θ is the scattering angle. Thus the maximum in the vicinity of $\Theta = 0°$ is a companion of the antisolar peak at $\Theta = 180°$. Since the antisolar peak at $\Theta = 180°$ is one of the reasons for the anthelion produced by 2-D plates and Parry columns, the difference in the intensity distribution around $\Theta = 0°$ between this study and that presented by Tränkle and Greenler[5] could be significant.

Discussion

Here we discuss the preceding point further. In the present study the factor $1/\sin\Theta$ has been included in the equation for the scattered intensity when converted to the scattered energy per unit solid angle. If we consider the externally reflected rays only, the phase function for randomly oriented hexagonal crystals is the same as that for spheres of the same refractive index discussed by van de Hulst,[13] in which the $1/\sin\Theta$ factor is included. The similarity of the phase functions for spheres and hexagonal crystals supports the validity of the factor $1/\sin\Theta$ in any cases of randomly oriented convex particles. Next let us consider horizontally oriented ice crystals. In Plate 3-13 of Ref. 2 the antisolar arcs are shown to cross the subparhelic circle and the antisolar peak in the case of Parry columns. These phenomena are reproduced in this study, as shown by Fig. 3(b). The antisolar peak would not appear if the factor $1/\sin\Theta$ were not taken into account in the computation. Thus the appearance of the antisolar peak indirectly confirms the necessity of this factor in the case of horizontally oriented crystals as well.

The externally reflected light pattern produced by 2-D columns around the light source can become diamondlike in shape. In order to demonstrate this, the transmitted light rays that undergo more than two internal reflections are suppressed to highlight the intensity generated by externally reflected rays. Since even a minor deformation of the ice crystal from the hexagonal shape modifies the directions of transmitted rays, rays that undergo more than two internal reflections are not likely to contribute to halo phenomena. Large and small diamond-shaped light patterns often show up in the vicinity of the Sun. Figures 6(a) and 6(b) approximately correspond to Plates 2-18 and 2-21 of Ref. 2. The reason for the large diamond shape is that more externally reflected rays are scattered to the solar principal ($\Phi = 0°$ and $180°$) and almucanter ($\Phi = 90°$ and $270°$) planes, where Φ is the azimuthal angle in reference to the solar principal plane. The factor $1/\sin\Theta$ has singularities at $\Theta = 0°$ and $180°$. For scattering angles close to these two angles, the scattered intensities due to reflections and refractions cannot be precisely computed. However, since all the optical phenomena occur at scattering angles greater than 1°, the present results should be adequate for their interpretation. As pointed out by Takano and Asano,[14] Fraunhofer-diffracted light could contribute to the inner intense diamond light pattern. However, it seems that the outer faint diamond shape is due primarily to the externally reflected light but not to the diffracted light. The relative contribution of diamond-shaped light patterns around the Sun due to the diffracted and externally reflected light rays is a subject that requires further study.

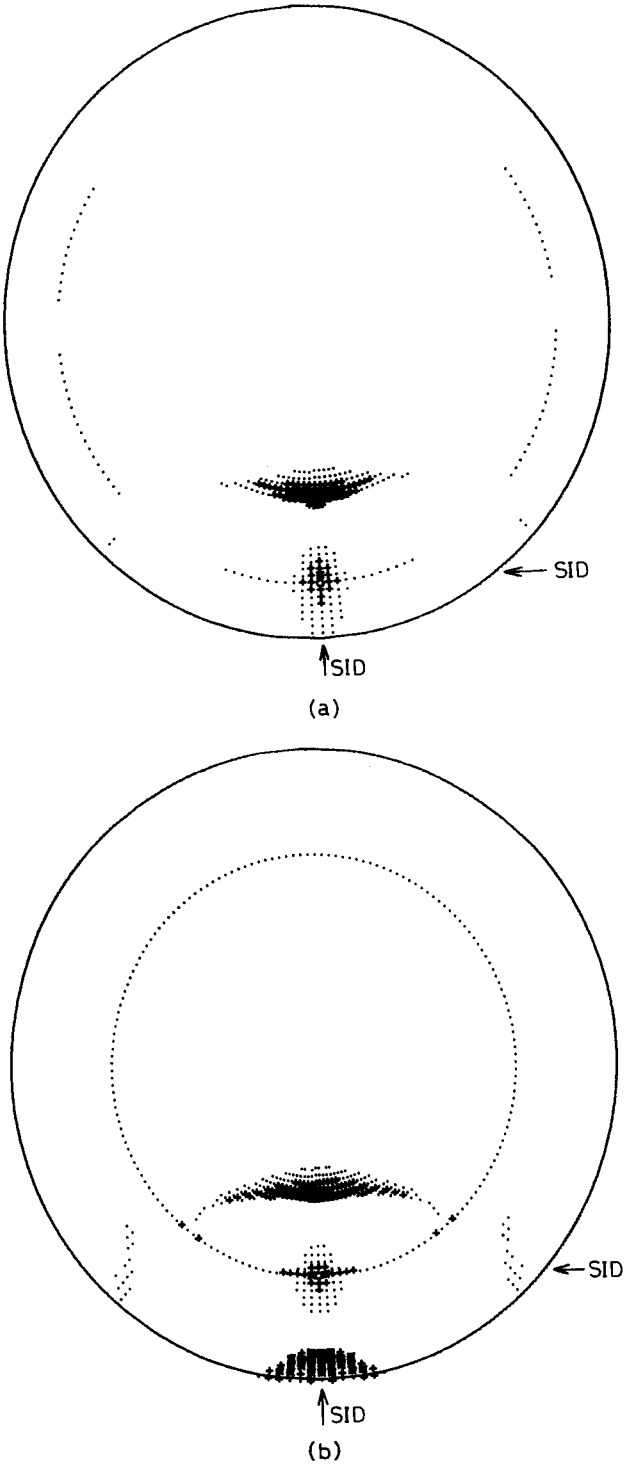

Fig. 6. (a) Intensity pattern for 2-D columns with $L/2a = 2.5$ at $\lambda = 0.55$ μm above the horizon. The solar zenith angle θ_0 is 73°. ·, +, *, and ■ denote 0, 1, 2, and 3, respectively, in units of $[2 \log_{10} P_{11}] - 2$ in order to enhance the pattern around the Sun. (b) Same as in (a) but for $L/2a = 1.5$ and $\theta_0 = 60°$ and in units of $[2 \log_{10} P_{11}] - 3$.

CONCLUDING REMARKS

We have presented, for the first time to our knowledge, the single-scattering patterns due to Parry and 2-D columns in the entire space. In the cases of Parry columns and 2-D plates, the anthelion can appear owing to the coupling of the subsun and the antisolar peak associated with double scattering. However, the anthelion can be produced by single scattering that involves 2-D columns. The anthelion has been observed by Evans and Tricker[15]: Fig. 1 of their paper, shows that 22° and 44° parhelia were observed, but the anthelic, or Parry, arc was absent. Thus the observed anthelion could be a result of the double-scattering effect of 2-D plates.

In addition to the well-known halo phenomenon produced by multiple scattering, we have shown that the 66° parhelion can be produced by 2-D plates. Moreover, uniform parhelic and circumzenithal circles are also simulated from the multiple-scattering program for optically thick cirrus clouds. Finally, we have discussed the possible causes of the diamond-shaped light pattern around the Sun in connection with the externally reflected and Fraunhofer-diffracted light rays.

ACKNOWLEDGMENTS

All the computations in this research were carried out on the San Diego Super Computer Cray X-MP/48. This research was supported in part by National Science Foundation grant ATM88-15712. We thank Christine Larrinaga for assistance in the preparation of this manuscript.

REFERENCES AND NOTES

1. R. A. R. Tricker, *Ice Crystal Haloes* (Optical Society of America, Washington, D.C., 1979).
2. R. G. Greenler, *Rainbows, Halos, and Glories* (Cambridge U. Press, New York, 1980).
3. F. Pattloch and E. Tränkle, "Monte Carlo simulation and analysis of halo phenomena," J. Opt. Soc. Am. A **1**, 520–526 (1984).
4. R. G. Greenler and E. Tränkle, "Anthelic arcs from airborne ice crystals," Nature (London) **311**, 339–343 (1984).
5. E. Tränkle and R. G. Greenler, "Multiple-scattering effects in halo phenomena," J. Opt. Soc. Am. A **4**, 591–599 (1987).
6. Y. Takano and K. N. Liou, "Solar radiative transfer in cirrus clouds. Part I. Single-scattering and optical properties of hexagonal ice crystals," J. Atmos. Sci. **46**, 3–19 (1989).
7. Y. Takano and K. N. Liou, "Solar radiative transfer in cirrus clouds. Part II. Theory and computation of multiple scattering in an anisotropic medium," J. Atmos. Sci. **46**, 20–36 (1989). There is a typographical error in this reference. $L/2a$ 4 μm/40 μm in the caption of Fig. 11 should be replaced with $L/2a = 8$ μm/80 μm.
8. E. A. Ripley and B. Saugier, "Photometers at Saskatoon on 3 December 1970," Weather **26**, 150–157 (1971).
9. Y. Takano and K. Jayaweera, "Scattering phase matrix for hexagonal ice crystals computed from ray optics," Appl. Opt. **24**, 3254–3263 (1985).
10. D. K. Lynch and Pt. Schwartz, "Origin of the anthelion," J. Opt. Soc. Am. **69**, 383–386 (1979).
11. G. H. Liljequist, "Halo phenomena and ice crystals," in *Norwegian-British-Swedish Antarctic Expedition, 1949–1952, Scientific Results* (Norsk Polarinstitutt, Oslo, 1956), Vol. 2, Part 2, p. 52.
12. W. J. Humphreys, *Physics of the Air* (Dover, New York, 1964).
13. H. C. van de Hulst, *Light Scattering by Small Particles* (Wiley, New York, 1957).
14. Y. Takano and S. Asano, "Fraunhofer diffraction by ice crystals suspended in the atmosphere," J. Meteorol. Soc. Jpn. **61**, 289–300 (1983).
15. W. F. J. Evans and R. A. R. Tricker, "Unusual arcs in the Saskatoon halo display," Weather **27**, 234–238 (1972).